Available online at www.sciencedirect.com
ScienceDirect
Catalysis Today 131 (2008) 270–277
CATALYSIS TODAY
www.elsevier.com/locate/cattod

Microstructure effect of carbon nanofiber on electrocatalytic oxygen reduction reaction

Jun-Sheng Zheng [a], Xin-Sheng Zhang [a,b,*], Ping Li [a], Xing-Gui Zhou [a], Wei-Kang Yuan [a]

[a] *UNILAB, State Key Laboratory of Chemical Engineering, East China University of Science and Technology, Shanghai 200237, China*
[b] *Shanghai Key Laboratory of Green Chemistry and Chemical Processes, Department of Chemistry, East China Normal University, Shanghai 200062, China*

Available online 3 December 2007

Abstract

Carbon nanofibers (CNFs) with controlled microstructures, i.e. platelet CNF (p-CNF), fish-bone CNF (f-CNF) and tube CNF (t-CNF), are synthesized, and their behaviors in electrocatalytic oxygen reduction reaction (ORR) in acid media are investigated in this paper. The physico-chemical properties of the CNFs are characterized by high resolution transmission electron microscope (HRTEM), N_2 adsorption–desorption and Raman spectrum. Cyclic voltammetry experiments show that the CNFs have higher ORR activities than graphite. The p-CNF, which has the highest ratio of edge atoms to basal atoms, demonstrates the most positive ORR onset potential and ORR peak potential. The f-CNF, which has the largest amounts of ORR active sites, exhibits the highest ORR peak current. The t-CNF demonstrates the most negative ORR onset potential, negative ORR peak potential, and the least ORR peak current, which is a result of the fewest catalytic active sites. Furthermore, the microstructures of CNFs can impact the reaction process. The ORR on p-CNF or f-CNF is controlled by diffusion, while the ORR on t-CNF is jointly controlled by surface reaction and diffusion.
© 2007 Elsevier B.V. All rights reserved.

Keywords: Carbon nanofiber; Microstructures; Oxygen reduction reaction; Electrocatalytic properties

1. Introduction

The oxygen reduction reaction (ORR) is involved in a number of electrochemical processes, such as metal corrosion, water electrolysis, and energy conversion/storage [1–3], and has been a research focus in recent decades when alternative resource utilization and energy conversion efficiency are of primary concern [2–5]. The ORR on carbon-based electrodes has been extensively studied, and different types of carbon materials, e.g. activated carbon (AC) [6], highly oriented pyrolytic graphite (HOPG) [7], glassy carbon (GC) [8], boron-doped diamond (BDD) [9], reticulated vitreous carbon (RVC) [10] and carbon nanotubes (CNTs) [11], are of wide research interest.

It is evident that the microstructures of carbon materials have significant influences on the ORR properties. Bennett et al. investigated the ORR on BDD electrode [12,13], and indicated that the sp^2 carbon impurities on BDD had obvious influences on the electrode reaction kinetics. Similarly, Yano et al. [9] found that the ORR on BDD was slightly inhibited when the catalytic functional groups on the electrode surface were deactivated by pretreatment. Ozaki et al. studied the ORR activity on the carbons prepared from ferrocene and poly (furfuryl alcohol) [14], and revealed that the carbons containing shell-like structures showed larger ORR activities than the carbons without shell-like structures.

The ORR on carbon materials was investigated both in alkaline and acid solution. In alkaline solution, most of carbon materials are active catalysts for oxygen reduction. Yang and McCreery [15] investigated the oxygen reduction on GC electrodes, and found that reduction of oxygen to superoxide on the GC surface covered with a covalently bonded methylphenyl monolayer was reversible above pH 10. The results also revealed that the ORR peak potential became more negative when the pH value decreased. However, in acid media, the ORR

* Corresponding author. Tel.: +86 21 64253469; fax: +86 21 64253528.
E-mail address: xszhang@ecust.edu.cn (X.-S. Zhang).

0920-5861/$ – see front matter © 2007 Elsevier B.V. All rights reserved.
doi:10.1016/j.cattod.2007.10.104

kinetics is slower than that on alkaline solution, and some researchers found that the ORR of carbon materials may be independent of pH value. For example, Sabirov and Tarasevich [6] showed that the ORR on pyrolytic graphite (PG) electrodes was independent of pH in the range from 1 to 4. Taylor and Humffray also found that the ORR on GC electrodes was independent of pH [16].

Carbon nanofibers (CNFs) have been intensively studied as catalyst materials during the last two decades for the possibility of tailoring their microstructures, such as the diameter, the graphite plane angle to the fiber axis, the ratio of edge atoms to basal atoms, etc., with certain preparation procedures [17–20]. Generally, CNFs can be divided into platelet CNF (p-CNF), tubular CNF (t-CNF) and fish-bone CNF (f-CNF) according to the different arrangement of graphene layers. The graphene layers of p-CNF are vertically to the fiber axis, and the exposed surfaces are mainly occupied by edge atoms, while the graphene layers of t-CNF are parallel to the fiber axis and many basal atoms are exposed. The graphene layers of f-CNF are inclining to the fiber axis, and the ratio of edge atoms to basal atoms can be adjusted by controlling the angle of graphene layers to the fiber axis.

Recently, CNFs are used as support for noble metal catalysts to improve the ORR activity. Bessel et al. [20] employed Pt/CNFs and Pt/(Vulcan XC-72) as the electrocatalysts for direct methanol fuel cell (DMFC), and found that the p-CNF and t-CNF were superior to f-CNF or Vulcan XC-72 in terms of ORR activity. They also showed that 5 wt% Pt supported on p-CNF or t-CNF would be as active as 25 wt% Pt supported on f-CNF or XC-72. Similarly, we found that Pd/p-CNF had a higher ORR activity than Pd/f-CNF or Pd/AC in a recent paper [21]. However, Ismagilov et al. [22] reported that the performance of electrocatalysts with CNFs as support was inferior to those with Vulcan XC-72 and amorphous supermicroporous carbons (ASC) as supports. These inconsistent results are most probably caused by the differences in CNFs properties, especially the lattice and surface structures of CNFs.

Since the inconsistent results were reported by different researchers, it is of importance to learn the microstructures effect of CNFs on the ORR performance. However, few results can be found from the literature dealing with this topic. In this study, CNFs with different microstructures were synthesized and characterized, and their ORR properties, i.e. ORR onset potential, ORR peak potential and peak current and reaction process, were investigated by cyclic voltammetry to provide more insight on the microstructures effect of the CNFs on the ORR.

2. Experimental

2.1. Catalyst preparation

CNFs with different microstructures, i.e. p-CNF, f-CNF and t-CNF, were synthesized by decomposition of CO on different catalysts, i.e. iron powder, Ni_3Fe_2/γ-Al_2O_3 and Ni/γ-Al_2O_3, in a fixed-bed quartz reactor by catalytic chemical vapor deposition (CCVD). For example, for p-CNF, one gram of the catalyst precursor containing Fe was placed in a horizontal quartz tube reactor of 40 mm i.d. and 500 mm length, and was then reduced in a flow of H_2 (40 ml/min) and Ar (120 ml/min) at 600 °C for 3 h. At the same temperature, CNFs started to grow when the gas flow was changed to a mixture of CO (40 ml/min) and H_2 (20 ml/min) and about 10 g CNFs were obtained in 16 h. The details of the synthesis procedure were also described in reference [19].

2.2. Preparation and modification of electrode

CNF or graphite powder was dispersed ultrasonically in a 0.5 wt% Nafion solution to obtain a homogenous black suspension with a concentration of 5 mg/ml. A 10 μl solution was pipetted onto the surface of a 3 mm diameter GC electrode. Before surface modification, the GC electrode was polished with 0.3 μm and 0.05 μm alumina slurries, washed by acetone, ethanol and water, and then subjected to ultrasonic agitation for 5 min in ultrapure water and dried in nitrogen flow. The surface modified electrode was dried at room temperature and in ambient air for 1 h and was washed with ultrapure water before use.

2.3. Purification of the as-grown CNFs

The metal impurities in the as-grown CNFs were removed electrochemically which was conducted by cyclic voltammetric scanning in 0.5 M $HClO_4$ electrolyte. The scan rate is 10 mV s^{-1}, and the scan range is from 0.60 V to 0.00 V vs. a saturated calomel electrode (SCE). The metal impurities in the as-grown CNFs were removed by the combination impact of potential scanning and acidic electrolyte. No metal oxidation or reduction current was found after electrochemical treatment, indicating that the metal impurities on the as-grown CNFs were removed effectively.

2.4. Catalyst characterization

The morphologies of the CNFs were characterized by high resolution transmission electron microscope (HRTEM, JEOL JEM 2010), and their textural properties were obtained from N_2 adsorption–desorption isotherms (ASAP 2010, Micromeritics, USA) at −196 °C. Specific surface areas were calculated with the Brunauer–Emmett–Teller equation, and the pore volumes and the pore size distributions were calculated with the Barrett–Joyner–Halenda method. Raman spectra was taken under ambient conditions using a Renishaw inVia + Reflex Raman spectrometer with an Ar-ion laser beam at an exciting radiation wavelength of 514.5 nm.

Electrochemical measurements were performed with an Autolab Potentiostat 30 electrochemical workstation (Eco Chemie B.V., The Netherlands) in a 0.5 M $HClO_4$ solution. The working electrode was GC that coated with CNF or graphite composite films. A platinum clump was used as a counter electrode, and a SCE was used as a reference electrode for all electrochemical measurements. All the potentials were reported versus the SCE reference electrode.

3. Results and discussion

3.1. Physico-chemical properties of CNFs

3.1.1. Morphology of CNFs

HRTEM micrographs of isolated CNFs are displayed in Fig. 1, which reveals that the graphene layers of CNFs are ordered with different angle to the fiber axis. The graphene layers of p-CNF are vertical to the fiber axis, while the graphene layers of f-CNF are about 30° inclining to the fiber axis and the graphene layers of t-CNF are parallel to the fiber axis. The diameters are also different, which is about 100 nm for p-CNF, obviously larger than that of f-CNF (about 50 nm) and t-CNF (about 30 nm).

3.1.2. Textural properties

Listed in Table 1 are the textural properties of CNFs. The textural properties of commercially available graphite, which was selected as a reference in this paper, are also presented in this table. The specific surface areas of CNFs are in the range of 86.6–204.7 m^2/g, which are obviously larger than that of graphite. The specific surface area of p-CNF is larger than that of f-CNF and t-CNF because the graphene layers of p-CNF are vertical to the fiber axis and some rough surfaces are formed [23].

Typical isotherms of N_2 adsorption–desorption of CNFs and graphite at cryogenic temperature are shown in Fig. 2, which appear principally as type IV, according the IUPAC classification and are very similar to those reported [24,25]. Hysteresis loops of H3 loop are marked on the isotherms for CNFs in Fig. 2, indicating the existence of a large amount of mesopores with a slit shape. These mesopores are mainly the interstices between entangled CNF filaments [20,21]. Table 1 and Fig. 2 also show that the micropores are very small and can be neglected, and the mesopores are the dominant pore structure for all CNFs. The mesopores can promote the diffusion, and this is a CNF's distinctive advantage for their application in electrocatalysis because the mass transportation is expedited.

3.1.3. Crystalline structures of CNF

Shown in Fig. 3 are the Raman spectra and their deconvolutions of p-CNF, f-CNF and t-CNF, which indicate the differences of CNF samples in crystalline structures. It is well known that the band near 1585 cm^{-1}, which is the predicted $E_{2gC=C}$ stretching vibrations and usually referred to the G-mode, is related to the basal atoms on CNFs. The band

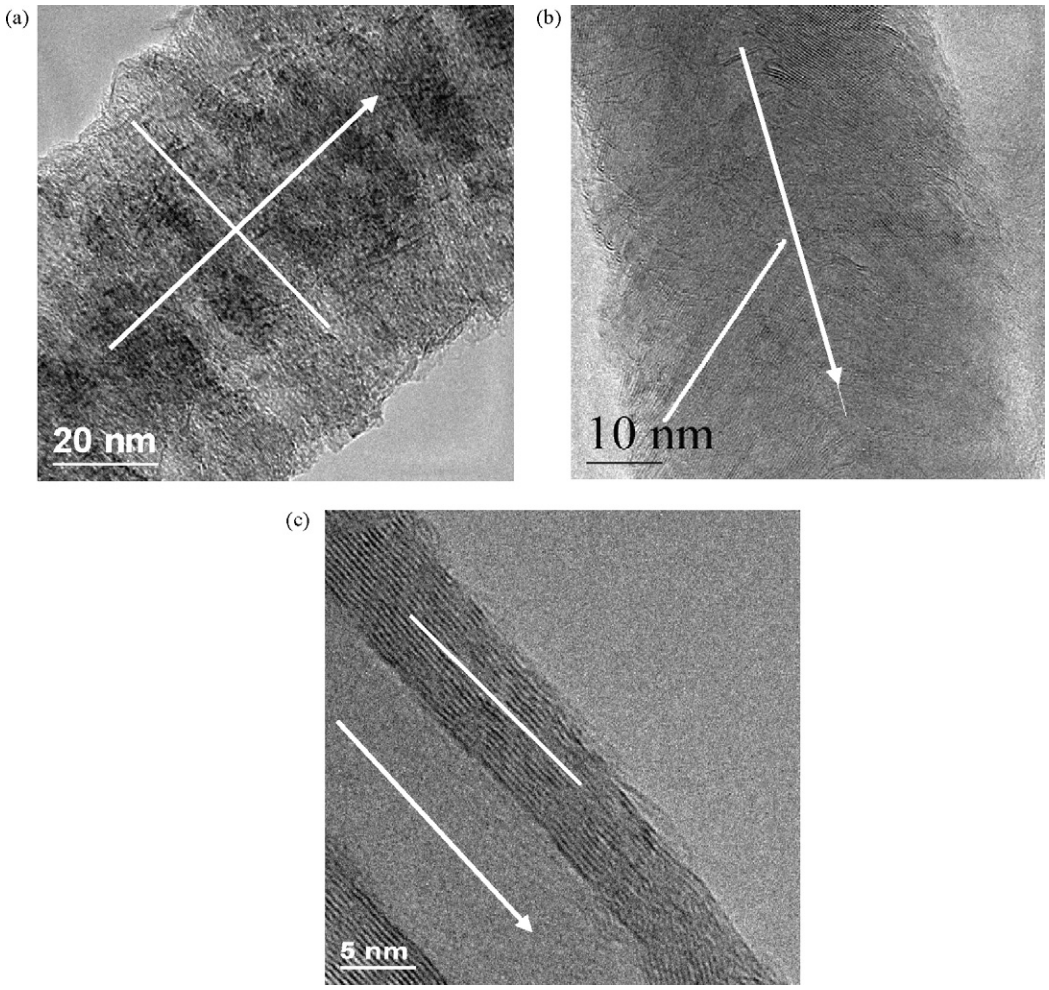

Fig. 1. HRTEM images of CNFs with different microstructures: (a) p-CNF, (b) f-CNF and (c) t-CNF.

Table 1
Properties of CNFs and graphite

Sample	Specific surface area (m^2/g)	Pore volume (cm^3/g)	Micropore volume (cm^3/g)	Diameter (nm)	Angle (°)
p-CNF	204.7	0.35	0.01	~100	90
f-CNF	86.6	0.30	0.00	~60	30
t-CNF	131.5	0.43	0.00	~30	0
Graphite	4.35	0.01	0.00	–	–

1345 cm^{-1}, the D-mode, is highly sensitive to graphitic defects within the graphene layers, and it is associated with the edge atoms on CNFs. Although the nature and origin of disorder are quite controversial in the literatures [25–27], it is established that integrated intensity ratio of 1345 cm^{-1}/1585 cm^{-1} (I_D/I_G) is, to some content, reflected the ratio of edge atoms to basal atoms [28,29]. The graphene planes of p-CNF are vertically to the fiber axis, and the exposed surface of p-CNF is mainly occupied by edge atoms, which can be attributed to the highest I_D/I_G value of p-CNF in the three CNF samples. The I_D/I_G value of f-CNF is smaller than that of p-CNF because the inclined graphene planes of f-CNF decrease the exposed density of edge atoms. The t-CNF exhibits the least value of I_D/I_G for the reason that the exposed surface is mainly occupied by basal atoms.

3.2. Effect of CNF microstructures on ORR properties

3.2.1. ORR onset reduction potential

As p-CNF, f-CNF and t-CNF have different morphologies, textural properties and crystalline structures, they may show different catalytic properties. To investigate the effect of CNF microstructures on ORR properties, cyclic voltammetric experiments were conducted. The electrolyte was first bubbled with nitrogen for 30 min to purge the oxygen, and the current–potential curve was recorded in the presence of nitrogen. Then the electrolyte was saturated with oxygen and the current–potential curve was also recorded. Fig. 4 depicts the ORR onset potentials of different carbon materials. Curve 1 and Curve 2 in Fig. 4 are the current–potential curves of the electrolyte saturated by nitrogen and oxygen, respectively. An evident reduction current appears in 0.28 V for p-CNF, while the ORR onset potentials of f-CNF and t-CNF are 0.15 V and 0.10 V, respectively. The reduction current increases when the potential decreases for the three CNF electrodes, suggesting that the reaction is in kinetic control region. Whereas for the graphite electrode, these two curves coincide with each other (Fig. 4d), implying the ORR onset potential of graphite is more negative than 0.00 V.

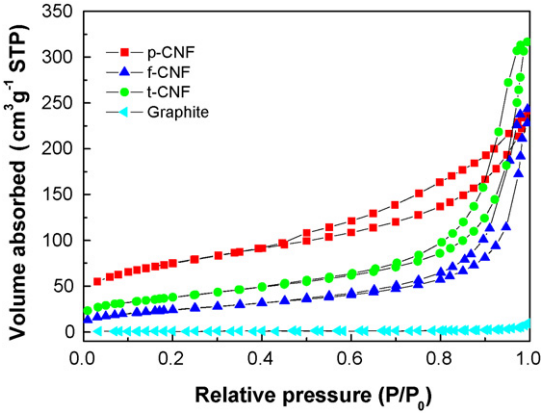

Fig. 2. N_2 adsorption–desorption curves of the CNFs and graphite.

Although the opinions on the ORR activity differences of carbon materials are conflicted in the literatures [30–32], their roots focalize on the microstructures of the carbon materials. Ajayan and co-workers [11] studied the ORR activities of CNT and graphite, and concluded that the CNT's activity higher than graphite was because of CNT contained some graphitic defects, e.g. pentagons derived defects at the CNT tips, and pentagon and heptagon derived defects in the graphitic lattice. Compared with graphite, CNF exposes more edge atoms. Those edge atoms contain a large number of ruptured chemical bonds, which possess a higher electron density than the π bonds on basal atoms and have a higher ability of releasing electrons. As a result, CNFs have higher ORR activities than graphite. The different ORR activities of CNFs are still caused by the differences in the ratio of edge atoms to basal atoms. The p-CNF has the highest ratio of edge atoms to basal atoms and shows the most positive ORR onset potential in the tested samples, while the ORR onset potential of t-CNF is the most negative because t-CNF has a lowest ratio of edge atoms to basal atoms among the three CNFs.

3.2.2. ORR peak potential and current

The differences in CNF microstructures not only influences ORR onset reduction potential, but also affects the ORR peak potential and peak current. Fig. 5 shows the cyclic voltammetric profiles of different electrodes at the scan rate of 10 mV/s, 25 mV/s, 50 mV/s, 75 mV/s, 100 mV/s and the scan range of 0.60 V to −0.60 V. The peak potentials and currents of different electrodes at the scan rate of 100 mV/s were also listed in Table 2.

The appearance of ORR peak is resulted from the deficiency of the reactant on the electrode surface. When the process is controlled by diffusion, the current will not increase further because of the shortage of the reactant on the electrode surface. The ORR peak potential of p-CNF at scan rate of 100 mV/s is −0.25 V, more positive than that of f-CNF (−0.27 V), t-CNF (−0.38 V) and graphite (−0.48 V). As proposed by Yeager [30], the reduction of oxygen in aqueous solution generally proceeds by either of two pathways. One is a direct four-electron pathway through which the molecular oxygen is

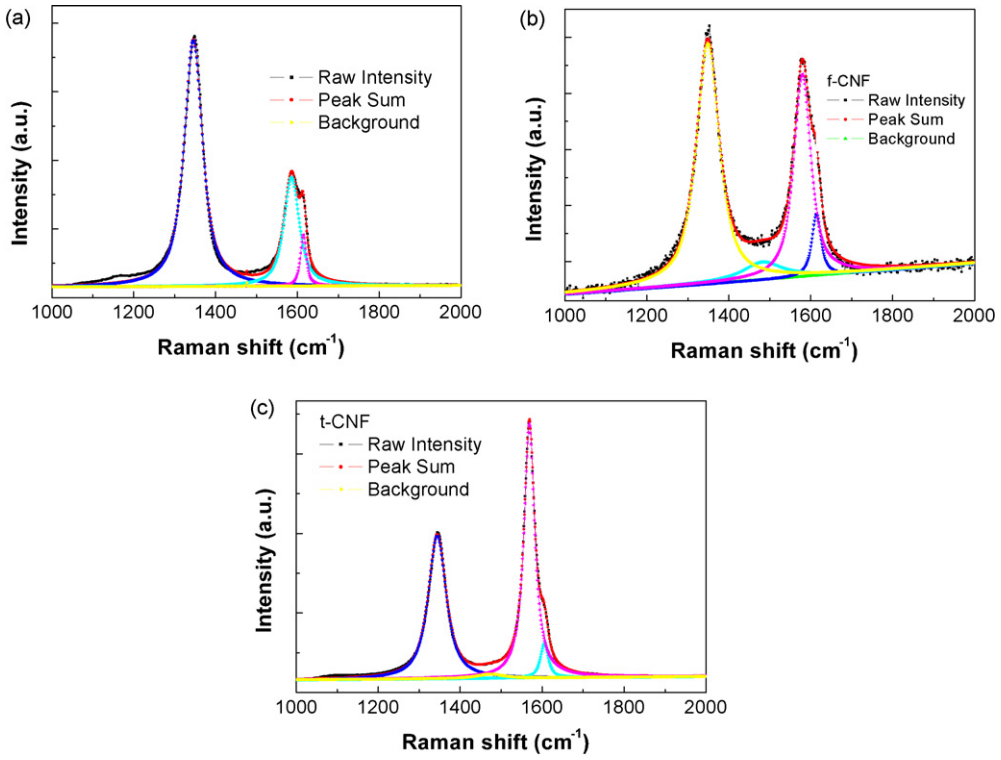

Fig. 3. Raman spectra and their deconvolutions of (a) p-CNF, (b) f-CNF and (c) t-CNF.

directly reduced to H_2O. The other is a peroxide pathway through which the molecular oxygen is firstly reduced to H_2O_2 and then to H_2O. For the carbon electrode, the mechanism of this reaction at different conditions has been extensively studied and it is generally accepted that in acidic and alkaline media oxygen reduction on carbon-based electrodes was a two-electron process [32–36]. Oxygen undergoes a $2e^-$ reduction, and peroxide can be formed as an intermediate according to

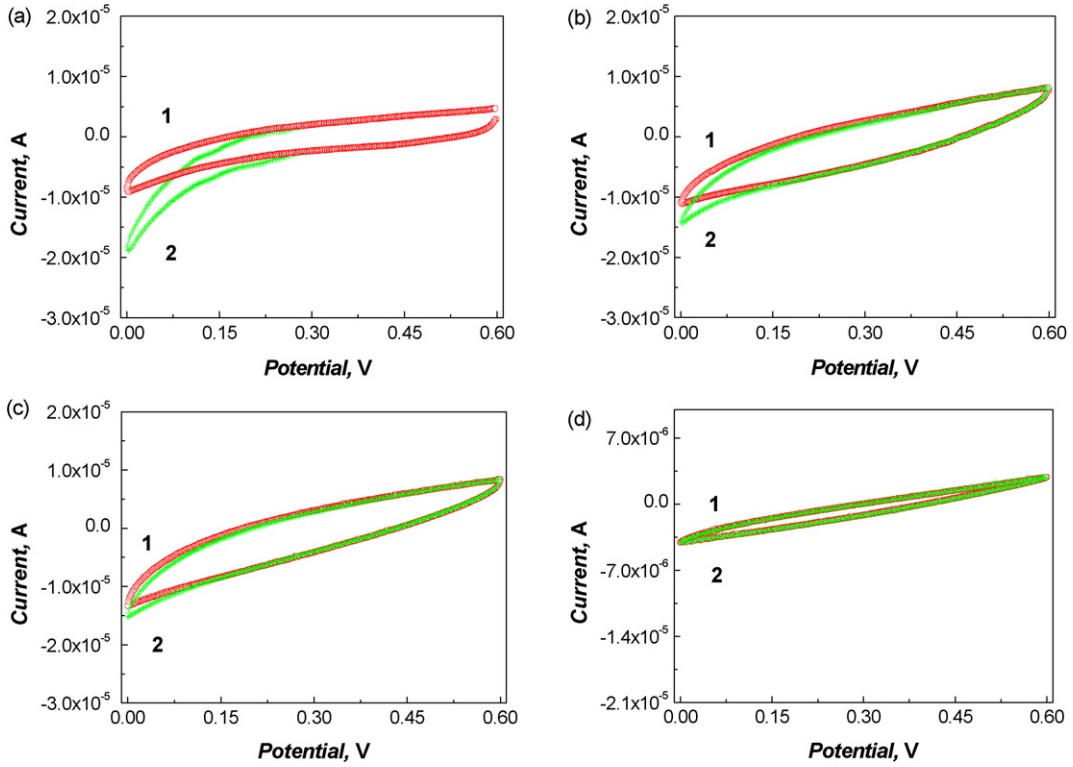

Fig. 4. Cyclic voltammetric analysis in 0.5 M $HClO_4$ solution saturated by nitrogen (1) and oxygen (2) at scan rate of 10 mV/s of (a) p-CNF, (b) f-CNF, (c) t-CNF and (d) graphite.

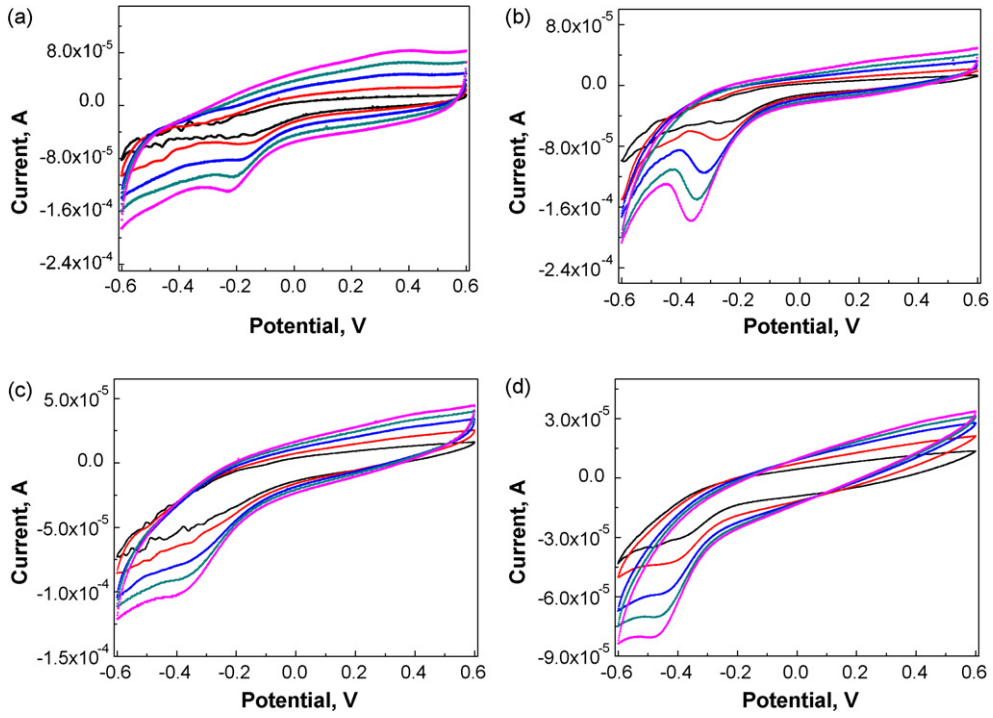

Fig. 5. Cyclic voltammetric analysis of oxygen reduction at different electrodes with different scan rates in oxygen saturated 0.5 M $HClO_4$ solution. The scan rates are 10 mV/s, 25 mV/s, 50 mV/s, 75 mV/s, and 100 mV/s from inside to outside, respectively. (a) p-CNF; (b) f-CNF; (c) t-CNF; (d) graphite.

Reaction (1).

$$O_2 + 2e^- + 2H^+ \rightarrow H_2O_2 \quad (1)$$

$$H_2O_2 + 2e^- + 2H^+ \rightarrow 2H_2O \quad (2)$$

Yang and McCreery [15] reported that the ORR peak of polished GC was at about −0.50 V at the scan rate of 100 mV/s at the pH value of 0, and this position is very close to the ORR peak potential of graphite (−0.48 V). Similarly, Chevalet et al. [37] reported an ORR peak potential of −0.49 V vs. Ag/AgCl for a $2e^-$ oxygen reduction process on a quinoline-modified mercury electrode.

To determine whether H_2O_2 was generated from the oxygen reduction, a small amount of KI-amylum solution was added to the fresh N_2 saturated electrolyte, the O_2 saturated electrolytes before and after electrolysis, respectively. The color of the electrolytes after electrolysis became blue in about 3 min, while the color of fresh N_2 saturated electrolyte and O_2 saturated electrolyte before electrolysis remained colorless within 30 min. These phenomena indicate the presence of H_2O_2 on the electrolyte after ORR, which was generated from the oxygen reduction. These results confirm that the ORR on the CNFs and graphite electrodes is a $2e^-$ process.

Since oxygen concentration is unchanged for all experiments, the ORR peak potential should be determined by the relative rate of diffusion and surface reaction when the scan rate remains the same. The surface reaction is associated with the activity of electrodes, while the diffusion is controlled by the textural properties of electrodes. Diffusion in mesopores is faster than in micropores, and the ORR peak potential for graphite would be more positive than CNFs if their intrinsic activities were the same. Obviously, graphite is much less active than CNFs because ORR peak potential of graphite is more negative than those of CNFs. The p-CNF has a mesopore volume relatively higher than f-CNF (Table 1), and the ORR peak potential of f-CNF would be more positive than that of p-CNF if these two catalysts had similar intrinsic activities. Since the ORR peak potential of p-CNF is more positive than that of f-CNF, one can believe that p-CNF has an ORR activity higher than f-CNF.

The ORR peak current is determined by the density of active sites of the catalyst. Graphite has the lowest density of active sites and therefore has the lowest ORR peak current. While the f-CNF has a ORR peak current of about −0.128 mA and is higher than that of p-CNF (−0.064 mA) and t-CNF (−0.048 mA), which can be explained by the smaller diameter of f-CNF than that of p-CNF and the higher ratio of edge atoms than that of t-CNF. Compared to f-CNF, p-CNF has more edge atoms, but the active site density (on weight basis) is smaller. As for the t-CNF, its active site density is the smallest among the three CNFs because its surface is mainly occupied by basal atoms.

Table 2
ORR peak potential and current of different CNF electrodes at the scan rate of 100 mV/s

Sample	Peak potential (V)	Peak current (mA)
p-CNF	−0.25	−0.064
f-CNF	−0.27	−0.128
t-CNF	−0.38	−0.048
Graphite	−0.48	−0.038

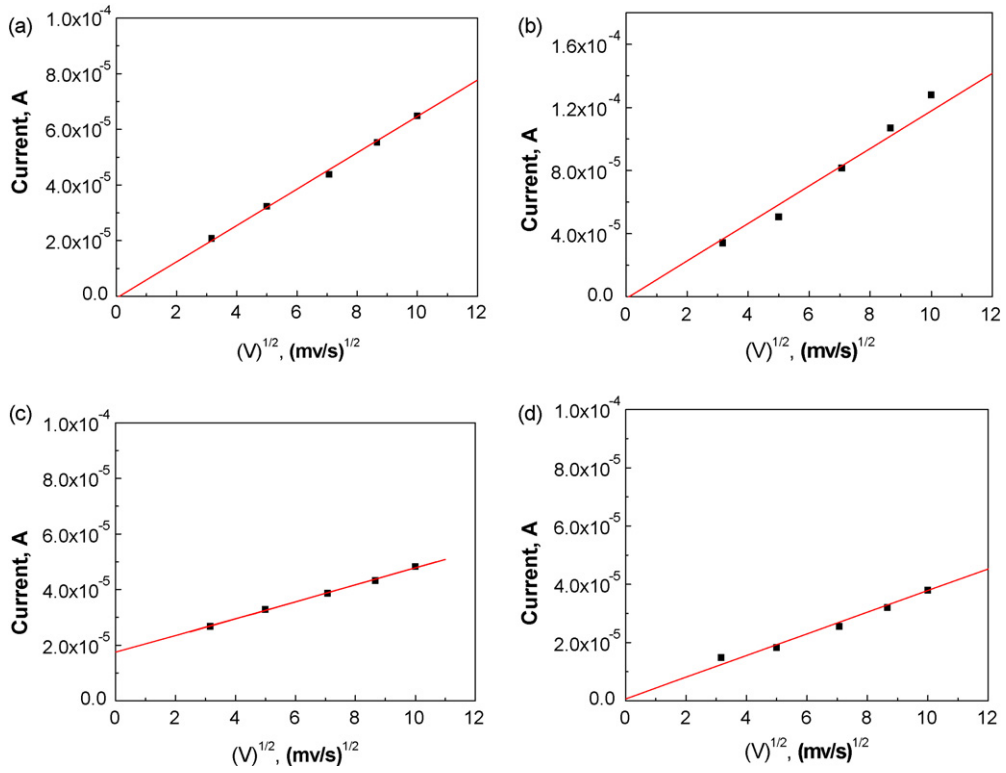

Fig. 6. The plot of the catalytic ORR peak currents as a function of the square root of scan rates (scan rates are 10 mV/s, 25 mV/s, 50 mV/s, 75 mV/s, 100 mV/s) at (a) p-CNF, (b) f-CNF, (c) t-CNF and (d) graphite.

3.2.3. Reaction process

As discussed previously, the microstructures of CNFs have significant influences on the ORR activity, ORR peak potential and peak current. They will also have influences on the behaviors of ORR process. Fig. 6 shows the ORR peak currents as a function of the square root of the scan rates of p-CNF, f-CNF, t-CNF and graphite, respectively. The lines in Fig. 6a, b and d pass through the origin of the coordinate axes, while the line in Fig. 6c does not, which indicates that the ORR process on p-CNF, f-CNF and graphite is diffusion-controlled, while the ORR process on t-CNF is jointly controlled by surface reaction and diffusion. This is because the ORR activity is high for p-CNF and f-CNF, while it is relative low for t-CNF. As for graphite, although it has the lowest ORR activity, the ORR process is still controlled by diffusion because of its small surface area and mesopore volume.

4. Conclusion

In this paper, three different CNFs, i.e. p-CNF, f-CNF and t-CNF, were used as ORR catalysts, and cyclic voltammetric experiments were carried out to investigate the influences of CNF microstructures on the ORR properties. The p-CNF has the highest ORR activity because it has a higher ratio of edge atoms to basal atoms. Although f-CNF has relative lower ratio of edge atoms to basal atoms than p-CNF, it has the highest ORR peak current for its higher density of catalytic activity sites. The t-CNF has the most negative ORR onset potential and the least ORR peak current for the lowest ratio of edge atoms to basal atoms. Moreover, the results show that the microstructures of CNFs can impact the ORR process. The ORR processes on p-CNF, f-CNF and graphite are controlled by diffusion, while the ORR on t-CNF is jointly controlled by surface reaction and diffusion.

Acknowledgements

The authors acknowledge the support from the Shanghai Key Laboratory of Green Chemistry and Chemical Processes (East China Normal University), the Raising State Key Laboratory of Green Chemistry Synthesis Technology (Zhejiang University of Technology), the NSFC/PetroChina major project (No. 20490200), and the special funding for the state key laboratories sponsored by the Science and Technology Committee of Shanghai Municipality, China (No. 036505010).

References

[1] R. Holze, W. Vielstich, J. Electrochem. Soc. 131 (1984) 2298.
[2] C.W. Walton, E.J. Rudd (Eds.), Energy and Electrochemical Processing for a Cleaner Environment, vol. 97-28, The Electrochemical Society, Pennington, NJ, 1997, p. 129.
[3] H. Arai, S. Muller, O. Haas, J. Electrochem. Soc. 147 (2000) 3584.
[4] N. Jia, R.B. Martin, Z. Qi, M.C. Lefebvre, P.G. Pickup, Electrochim. Acta 46 (2001) 2863.
[5] Y.Q. Chu, Ph.D. Thesis, Zhejiang University of Technology, 2004.
[6] F.Z. Sabirov, M.R. Tarasevich, Elektrokhimiya 5 (1969) 608.
[7] A. Sarapuu, K. Helstein, D.J. Schiffrin, K. Tammeveski, Electrochem. Solid-State Lett. 8 (2005) E30.
[8] J. Maruyama, I. Abe, J. Electroanal. Chem. 527 (2002) 65.

[9] T. Yano, E. Popa, D.A. Tryk, K. Hashimoto, A. Fujishima, J. Electrochem. Soc. 146 (1999) 1081.
[10] J.M. Friedrich, C. PoncedeLeón, J. Electroanal. Chem. 561 (2004) 203.
[11] P.J. Britto, K.S.V. Santhanam, A. Rubio, A. Alonso, P.M. Ajayan, Adv. Mater. 11 (1999) 154.
[12] D.A. Tryk, C.R. Cabrera, A. Fujishima, N. Spataru, Fundamental Understanding of Electrode Processes, in Memory of Professor Ernest B Yeager, The Electrochemical Society Proceedings, Pennington, New Jersey, 2005, 12–16 Oct. 2003, paper No. 3.
[13] J.A. Bennett, J. Wang, Y. Show, G.M. Swain, J. Electrochem. Soc. 151 (2004) E306.
[14] J.I. Ozaki, K. Nozawa, K. Yamada, Y. Uchitama, Y. Yoshimoto, A. Furuichi, T. Yokoyama, A. Oya, L.J. Brown, J.D. Cashion, J. Appl. Electrochem. 36 (2006) 239.
[15] H.H. Yang, R.L. McCreery, J. Electrochem. Soc. 147 (2000) 3420.
[16] P. Serp, M. Corrias, P. Kalck, Appl. Catal. A 253 (2003) 337.
[17] R.J. Taylor, A.A. Humffray, J. Electroanal. Chem. Interfacial Electrochem. 64 (1975) 85.
[18] Z.J. Sui, Ph.D. Thesis, East China University of Science Technology, 2005.
[19] T.J. Zhao, Ph.D. Thesis, East China University of Science Technology, 2004.
[20] C.A. Bessel, K. Laubernds, N.M. Rodriguez, R. Baker, K. Terry, J. Phys. Chem. B 105 (2001) 1115.
[21] J.S. Zheng, X.S. Zhang, P. Li, J. Zhu, X.G. Zhou, W.K. Yuan, Electrochem. Commun. 9 (2007) 895.
[22] Z.R. Ismagilov, M.A. Kerzhentsev, N.V. Shikina, A.S. Lisitsyn, L.B. Okhlopkova, C.N. Barnakov, M. Sakashita, T. Iijima, K. Tadokoro, Catal. Today 102–103 (2005) 58.
[23] P. Li, T. Zhao, J. Zhou, Z. Sui, Y. Dai, W. Yuan, Carbon 43 (2005) 2701.
[24] T.V. Reshetenko, L.B. Avdeeva, V.V. Pushkarev, S.V. Cherepanova, A.L. Chuvilin, V.A. Likholobov, Z.R. Ismagilov, Carbon 41 (2003) 1605.
[25] W. Yan, D.C. Alsmeyer, R.L. McCreery, Chem. Mater. 2 (1990) 557.
[26] N. Keller, N.I. Maksimova, V.V. Roddatis, M. Schur, G. Mestl, Y.V. Butenko, V.L. Kutznetov, R. Schlogl, Angew. Chem. Int. Ed. 41 (2002) 1885.
[27] S. Maldonado, K.J. Stevenson, J. Phys Chem. B 108 (2004) 11375.
[28] T.G. Ros, A.J. van Dillen, J.W. Geus, D.C. Koningsberger, Chem. Eur. J. 8 (2002) 1151.
[29] Y. Otake, R.G. Jenkins, Carbon 31 (1993) 109.
[30] E. Yeager, J. Mol. Cat. 38 (1986) 5.
[31] M. Apple, A.J. Appleby, Electrochim. Acta 23 (1978) 1243.
[32] A.J. Appleby, Electrochim. Acta 37 (1993) 117.
[33] F.Z. Sabirov, M.R. Tarasevich, R.K. Burshtein, Elektrokhimiya 6 (1970) 1130.
[34] T. Nagaoka, T. Sakai, K. Ogura, T. Yoshino, Anal. Chem. 58 (1986) 1953.
[35] S. Maldonado, K.J. Stevenson, J. Phys. Chem. B 109 (2005) 4707.
[36] R.A. Sidik, A.B. Anderson, N.P. Subramanian, S.P. Kumaraguru, B.N. Popov, J. Phys. Chem. B 110 (2006) 1787.
[37] J. Chevalet, F. Rouelle, L. Gierst, J.P. Lambert, J. Electroanal. Chem. 39 (1972) 201.